LEARNING WHAT AND WHERE TO ATTEND

Anonymous authors
Paper under double-blind review

ABSTRACT

Most recent gains in visual recognition have originated from the inclusion of attention mechanisms in deep convolutional networks (DCNs). Because these networks are optimized for object recognition, they learn where to attend using only a weak form of supervision derived from image class labels. Here, we demonstrate the benefit of using stronger supervisory signals by teaching DCNs to attend to image regions that humans deem important for object recognition. We first describe a large-scale online experiment (ClickMe) used to supplement ImageNet with nearly half a million human-derived "top-down" attention maps. Using human psychophysics, we confirm that the identified top-down features from ClickMe are more diagnostic than "bottom-up" saliency features for rapid image categorization. As a proof of concept, we extend a state-of-the-art attention network and demonstrate that adding ClickMe supervision significantly improves its accuracy and yields visual features that are more interpretable and more similar to those used by human observers.

1 INTRODUCTION

Attention has become the subject of intensive research within the deep learning community. While biology is sometimes mentioned as a source of inspiration (Stollenga et al., 2014; Mnih et al., 2014; Cao et al., 2015; You et al., 2016; Chen et al., 2017; Wang et al., 2017; Biparva and Tsotsos, 2017), the attentional mechanisms that have been considered remain limited in comparison to the rich and diverse array of processes used by the human visual system (see Itti et al., 2005, for a review). In addition, whereas human attention is driven by varying task demands, attention networks are solely optimized for object recognition. This means that, unlike infants who can rely on a myriad visual cues to learn to focus their attention (Itti et al., 2005), DCNs must solve the challenging problem of learning where to attend from weak supervisory signals derived from statistical associations between image pixels and class labels. Here, we investigate how explicit human supervision – teaching DCNs where to attend – affects their performance and interpretability.

1.1 RELATED WORK

Attention models in neuroscience Work in computational neuroscience has posited that there are two main pathways that guide visual attention (Torralba et al., 2006). *Global features* are typically used to compute so-called "summary statistics" by averaging activities from individual feature channels across the entire scene. These representations are designed to capture the scene layout or "gist", and are hypothesized to capture contextual information that guides attention to task-relevant features (Oliva and Torralba, 2007). This is most similar to the feature-based attention that is used in most state-of-the-art networks (Bell et al., 2016; Wang et al., 2017; Hu et al., 2017). A complementary form of attention known as visual saliency (Itti and Koch, 2001) is derived from *local feature* representations, and is speculated to act as a task-independent topographical encoding of feature conspicuity in a visual scene. It has been proposed that the rapid convergence of these two pathways acts as an efficient shortcut for filtering clutter from object detection processes (Torralba et al., 2006).

Attention networks In addition to extensive work aimed at explicitly predicting human eye fixations and/or detecting objects (see Nguyen et al., 2018, for a review), recent research on image categorization has focused on integrating attention modules within end-to-end trainable deep network architectures. These attention modules fall into two broad categories that are conceptually similar to

the global and local pathways studied in visual neuroscience. *Feature-based attention* (also called "channel-wise" attention) involves learning a task-specific modulation that is applied across an entire scene to adjust feature maps. *Spatial attention* is a complementary form of attention which involves learning a spatial mask that enhances/suppresses the activity of units inside/outside a "spotlight" positioned over a scene. This is done according to units' spatial location independently of their feature tuning. Such mechanisms have been shown to significantly improve performance on visual question answering and captioning (e.g., Nam et al., 2017; Patro and Namboodiri, 2018). Here, we combine spatial- and feature-based attention into a single mask that modulates feature representations, similarly to state-of-the-art approaches (e.g., Chen et al., 2017; Wang et al., 2017; Biparva and Tsotsos, 2017; Park et al., 2018; Jetley et al., 2018), with a formulation that additionally supports supervision from human annotations.

Humans-in-the-loop computer vision A central goal of the present study is to leverage human supervision to co-train an attention network. Previous work has shown that it is possible to augment vision systems with human perceptual judgments on many difficult recognition problems (e.g., Vondrick et al., 2015; Shanmuga Vadivel et al., 2015; Kovashka et al., 2016; Deng et al., 2016). In particular, online games, especially multi-player games, constitute an efficient way to collect high-quality human ground-truth data (e.g., von Ahn et al., 2006; Deng et al., 2016; Das et al., 2016; Linsley et al., 2017). In a two-player game, an image may be gradually revealed to a "student" tasked to recognize it, by a remote "teacher" who draws "bubbles" on screen to unveil specific image parts (Linsley et al., 2017). The gameplay mechanics introduced by assembling teams of players reduces annotation noise in these games, but also limits their suitability for large-scale data collection. This limitation is aleviated in one-player games (Deng et al., 2013; 2016; Das et al., 2016), where a player may be asked to sharpen regions of a blurred image to answer questions about it. The game introduced here differs from these earlier studies (Linsley et al., 2017) in that it has a human player collaborate with a DCN to discover important visual features for recognition at ImageNet scale.

Attention datasets Recording eye fixations while viewing a stimulus is a classic way to explore visual attention (e.g., Judd et al., 2009). It is, however, difficult and costly to acquire large-scale eye tracking data, leading researchers instead to track computer mouse movements during task-free image viewing. Maps collected from individual observers can then be combined into a single "bottom-up" saliency map, as is done for the popular Salicon dataset (Jiang et al., 2015). Still, Salicon contains saliency maps for 10k images, which is probably at least one order of magnitude short of the number of samples needed for co-training a deep network in object recognition. We instead describe a gamification procedure used to collect nearly a half-million "top-down" (task-driven) attention maps over several months. As we demonstrate through psychophysics, our top-down attention maps collected as human observers are actively identifying maximally informative visual features for object categorization better reflect their recognition strategy than Salicon (section 2.2).

1.2 Contributions

Our contributions are three-fold: (i) We describe the large-scale online experiment `ClickMe.ai` to supplement ImageNet with nearly a half-million top-down attention maps derived from human participants. These maps are validated using human psychophysics and shown to be more diagnostic than bottom-up attention maps for rapid visual categorization. (ii) As a proof of concept, we describe an extension of the leading squeeze-and-excitation (SE) module, which we call the global-and-local attention (GALA) module because it combines global contextual guidance with local saliency. This extension yields substantial gains in accuracy on ILSVRC12. (iii) Incorporating ClickMe supervision leads to an even larger gain in accuracy while also creating visual representations that are more interpretable and more similar to those derived from human observers. By supplementing ImageNet with the public release of ClickMe attention maps, we hope to spur interest in the development of network architectures that are not only more robust and accurate, but also more interpretable and consistent with human vision.

2 ClickMe.ai

A large-scale effort is needed to gather sufficient attention annotations for training neural network models. Our starting point for this endeavor is the Clicktionary game introduced by Linsley et al.

(2017), which pairs online human participants to cooperatively annotate object images. This two-player game was successfully used to collect attention maps for a few hundred images, but we found it impossible to scale beyond that because of the challenge of matching pairs of players. These limitations prompted us to develop `ClickMe.ai`, an adaptation of Clicktionary into a single-player game that supports large-scale data acquisition. Indeed, ClickMe successfully ran for several months and produced nearly a half-million attention maps.

ClickMe consists of rounds of game play where human participants play with DCN partners to recognize images from the ILSVRC12 challenge. Players viewed object images and were instructed to use the mouse cursor to "paint" image parts that are most informative for recognizing its category (written above the image). Once the participant clicked on the image, 14×14 pixel bubbles were placed wherever the cursor went until the round ended (Fig. 1). Having players annotate in this way forced them to carefully monitor their bubbling while also preventing fastidious strategies that would produce overly sparse salt-and-pepper types of maps.

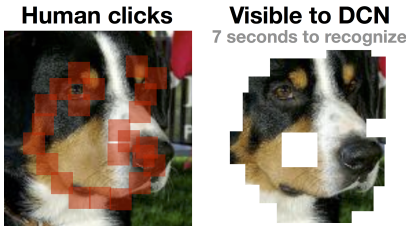

Figure 1: The ClickMe interface for human participants and their DCN partners. Participants select important image parts with their mouse by "painting" translucent bubbles on screen. At the same time, image parts of roughly double the size are shown to a DCN partner, tasked to recognize the image. Each round lasts until the DCN recognizes the object or if 7 seconds have passed (the latter occurred 47% of the time).

As players bubbled object parts they deemed important for recognition, a DCN tried to recognize a version of the image where only these bubbled parts were visible. We tried to make the game as entertaining and fast-paced as possible to maximize the number of rounds played by the human players. Hence, we nearly doubled the size of the bubbled regions shown to the DCN (21×21 pixels) to make sure that the objects would be visible to the DCN within a few seconds of play (Fig. 1). Thus, we do not expect the precise bubble locations to influence the timing or the accuracy of the DCN response. The reason for keeping a DCN in the loop (as opposed to a random timer) was (1) to make the game entertaining, and (2) to discourage human players from bubbling random locations in an image which are potentially unrelated to the object. Indeed, we have incorporated all the images used in Clicktionary (graciously provided by Linsley et al., 2017) and found that ClickMe maps are strongly correlated with Clicktionary maps (see Appendix). This suggests that the use of a DCN as a player did not bias the collected annotations, but it did allow us to collect human data at a scale suitable for co-training a DCN with human attention annotations.[1] A timer controlled the number of points participants received per image, and high-scoring participants were awarded prizes (see Appendix). Points were calculated as the proportion of time left on the timer after the DCN achieved top-5 correct recognition for the image. If the player could not help the DCN recognize the object within 7 seconds, the round ended and no points were awarded.

2.1 Game statistics

Data collection efforts on `ClickMe.ai` drew 1,235 participants (unique user IDs) who played an average of 380 images each. In total, we recorded over 35M bubbles, producing 472,946 ClickMe maps on 196,499 unique images randomly selected from our preparation of ILSVRC12 (see Appendix for details). All ClickMe maps were used in subsequent experiments, regardless of the ability of the DCN partner to correctly identify them within the time limit of a round. Fig. 2A shows sample ClickMe maps where pixel opacity is set according to how many times a bubble was overlaid on them over all rounds of game play where these images were presented. The maps typically highlight local image features, emphasizing certain object parts over others. For instance, ClickMe maps for animal categories (Fig. 2A, top row) are nearly always oriented towards facial components even when these are not prominent (e.g., snakes). In general, we also found that ClickMe maps for inanimate objects (Fig. 2A, bottom row) tended to exhibit a front-oriented bias, with distinguishing parts such

[1] Also see Appendix for an extended discussion about why it is unlikely that human observers were able to adopt a strategy that would be optimal for a DCN as opposed to selecting object features that they deemed important for recognition.

as engines, cockpits, and wheels receiving special attention. Additional game information, statistics and ClickMe maps are available as Appendix.

2.2 CLICKME AND OBJECT RECOGNITION

Rapid vision experiments have classically been used in visual neuroscience to probe visual responses while controlling for feedback processing (Serre et al., 2007; Thorpe et al., 1996; Eberhardt et al., 2016). Here, we devised such a rapid vision classification experiment to compare the contribution of top-down ClickMe features for object recognition with features derived from bottom-up image saliency (Figure 2B), closely following the approach of (Eberhardt et al., 2016). If human participants were more effective at recognizing object images based on ClickMe features than bottom-up saliency features, we reasoned it would validate the ClickMe approach and demonstrate the relevance of the collected feature importance maps to object recognition.

Our design of this experiment followed the rapid visual categorization paradigm used in Eberhardt et al. (2016) where stimuli are flashed and responses are forced to be rapid (under 550 ms; see Appendix for details). We recruited 120 participants from Amazon Mechanical Turk (`www.mturk.com`), each of whom viewed images that were masked to reveal a randomly selected amount of their most important visual features. Participants were organized into two groups ($N = 60$ participants in each): one which viewed images that were masked according ClickMe maps, and the other viewed images that were masked according to bottom-up saliency.

We tested participant responses on 40 target (animal) and 40 distractor (non-animal) images gathered from the Salicon (Jiang et al., 2015) subset of the Microsoft COCO 2014 (Lin et al., 2014) because it includes bottom-up saliency maps derived from human observers. Images were presented to human participants either intact or with a phase scrambled perceptual mask which selectively exposed their most important visual features according to attention maps derived from either ClickMe or Salicon. Attention maps from both resources were preprocessed so that there was spatial continuity for the pixels covering their most-to-least important visual features. This ensured that a low-level difference between attention maps, such as the presence of many discontinuous visually important regions, did not bias participants' responses in this rapid categorization experiment. Preprocessing was done with a novel "stochastic" flood-fill algorithm that relabeled attention map pixels with a score that combined their distance from the most important pixel with their labeled importance (see Appendix for details). Next, we created versions of each image that revealed between 1% and 100% (at log-scale spaced intervals) of its most important pixels.

This experiment measured how increasing the proportion of important visual features from either ClickMe or Salicon attention maps influenced behavior (see thumbnails in 2A for examples of images where 100% of ClickMe or Salicon features were revealed). Experiment results are shown in Fig. 2B: Human observers reached ceiling performance when 40% of the ClickMe features were visible (6% of all image pixels). In contrast, human observers viewing images masked according to Salicon required as much as 63% of these features to be visible, and did not reach ceiling performance until the full image was visible (accuracy measured from different participant groups). These findings validate that visual features measured by ClickMe are distinct from bottom-up saliency and sufficient for human object recognition.

3 PROPOSED NETWORK ARCHITECTURE

We designed the *global-and-local attention* (GALA) block as a circuit for learning complex combinations of local saliency and global contextual modulations that can optionally be supervised by ClickMe maps. The rational for this design, in particular the parallel attention pathways, is grounded in visual neuroscience, which is detailed in Related Work. Below we sketch the main computational elements of the architecture, and describe the process by which it is used to modulate activity at a layer in a DCN model (see Fig. 3 for a high-level overview of GALA attention transforming the DCN layer activity $\mathbf{U}$ into $\mathbf{U}'$ with the derived attention activity $\mathbf{A}$).

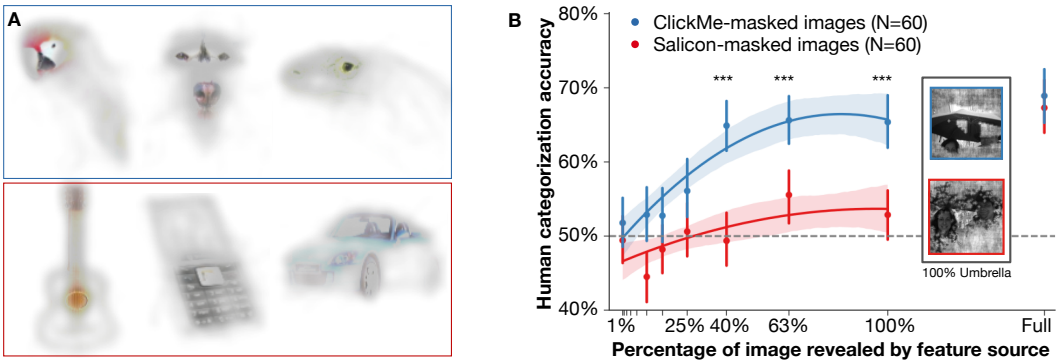

Figure 2: **(A)** A representative selection of ILSVRC12 images and their ClickMe maps. The transparency channel of select images reflect the fraction of ClickMe bubbles for that location across participants. Image features consistently deemed important for recognition are opaque and unimportant ones are transparent. Animals are outlined in blue and non-animals in red. **(B)** Features identified in "top-down" ClickMe maps are more diagnostic for object recognition than those identified in "bottom-up" Salicon maps. A rapid visual categorization experiment compared human performance in detecting animals when features were revealed according to ClickMe maps (blue curve) or Salicon maps (red curve). ClickMe- and Salicon-masked image exemplars are shown for the condition in which 100% of important features are visible, demonstrating how "bottom-up" saliency is not necessarily relevant to the task. For clarity, we omitted data between 1-10% of features visible from this plot where accuracy was chance for participants of both groups. Error bars are S.E.M. ***: p <0.001 (statistical testing with randomization tests (Edgington, 1964); see Appendix details).

3.1 Architecture

GALA modulates an input layer activity $\mathbf{U}$ with an attention mask $\mathbf{A}$ of the same dimension as the input, which captures a combination of global and local forms of attention. Here, the spatial height, width, and number of feature channels are denoted as H, W, and C s.t. $\mathbf{U}, \mathbf{A} \in \mathbb{R}^{H \times W \times C}$.

We begin by describing global attention in the GALA, which is based on the SE module (Hu et al., 2017). Global attention is denoted F_{global} in our model and yields the global feature attention vector $\mathbf{g} \in \mathbb{R}^{1 \times 1 \times C}$ (Fig. 3). This procedure involves two steps: first, calculating per-channel "summary statistics"; and second, applying a multilayer perceptron (MLP) transformation to shrink and then expand the dimensionality of these statistics. Summary statistics are computed with a global average applied to the vector $\mathbf{U} = [\mathbf{u}_k]_{k=1 \ldots C}$ to yield the vector $\mathbf{p} = (p_k)_{k=1 \ldots C}$. That is, $\mathbf{p_k} = \frac{1}{WH} \sum_{x=1}^{W} \sum_{y=1}^{H} \mathbf{u}_{kxy}$. This is followed by a two-layer MLP to shrink and then expand the dimensionality of $\mathbf{p}$, along with an intervening nonlinearity for learning complex dependencies between channels. The shrinking operation of this MLP ("squeeze" from Hu et al., 2017) is applied to the vector $\mathbf{p}$ by the operator $W_{shrink} \in \mathbb{R}^{\frac{c}{r} \times C}$, mapping it into a lower dimensional space. This is followed by an expansion operation ("excite" from Hu et al., 2017) $W_{expand} \in \mathbb{R}^{C \times \frac{c}{r}}$ (bias terms are omitted for simplicity) back to the original, higher dimensional space s.t. $\mathbf{g} = W_{expand}(\delta(W_{shrink}(\mathbf{p})))$. We set δ to be a rectified linear function (ReLU) and the dimensionality "reduction ratio" r of the shrinking operation to 4.

In addition to the SE/global attention module, we consider a local saliency module F_{local} for computing the local feature attention vector S (Fig. 3) as $S = \mathbf{V}_{collapse} * (\delta(\mathbf{V}_{shrink} * \mathbf{U}))$. Here, convolution is denoted with $*$, $\mathbf{V}_{shrink} \in \mathbb{R}^{1 \times 1 \times C \times \frac{c}{r}}$, and $\mathbf{V}_{collapse} \in \mathbb{R}^{1 \times 1 \times \frac{c}{r} \times 1}$. This is reminiscent of the local computations performed in computational-neuroscience models of visual saliency to yield per-channel conspicuity maps that are then combined into a single saliency map (Itti and Koch, 2001).

Outputs from the local and global pathways are integrated with $F_{integrate}$ to produce the attention volume $\mathbf{A} \in \mathbb{R}^{H \times W \times C}$. Because it is often unclear how tasks benefit from one form of attention vs. another, or whether task performance would benefit from additive vs. multiplicative combinations, $F_{integrate}$ learns parameters that govern these interactions. The vector $(a_c)_{c \in 1..C}$ controls

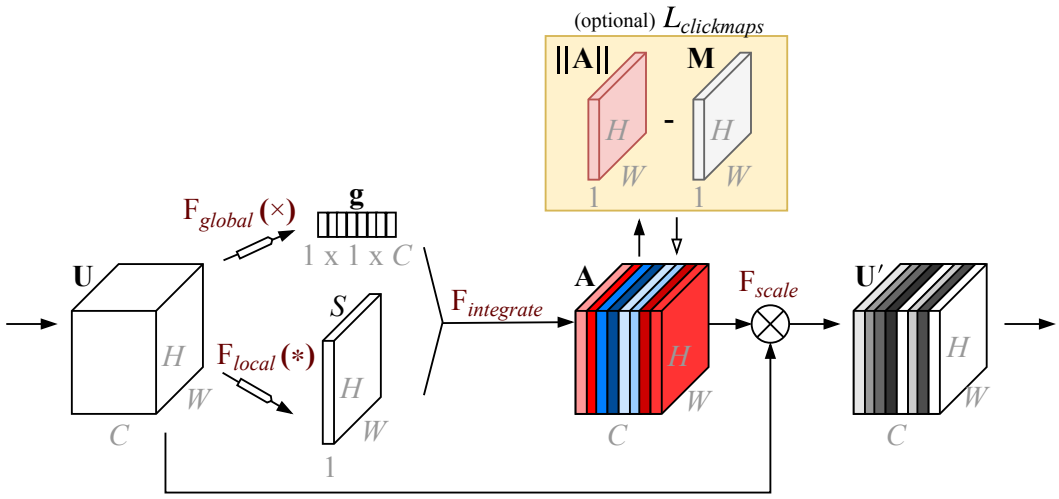

Figure 3: The global-and-local (GALA) module learns to combine local saliency with global contextual signals to guide attention towards image regions that are diagnostic for object recognition. The diagram here depicts a GALA applied to the activity from a convolutional layer in a deep network model, **U**. Information in the diagram flows from left to right, and **U** is processed with separate local (F_{local}) and global (F_{global}) operators to derive the local- and global-attention activity, which is integrated into the attention activity **A**. Attention is applied to the original activity, **U**, with elementwise multiplication (F_{scale}), to yield $\mathbf{U}'$. A GALA module can optionally be supervised by ClickMe maps (**M** in the yellow box), through an additional loss $\mathbf{L}_{clickmaps}$, which drives attention to visual features favored by humans (see Section 4 for details).

the additive combination of S and $\mathbf{g}$ per-channel, while $(m_c)_{c \in 1..C}$ does the same for their multiplicative combination. In order to combine attention activities $\mathbf{g}$ and S, they are first tiled to produce $\boldsymbol{G}^*, \boldsymbol{S}^* \in \mathbb{R}^{H \times W \times C}$. Finally, we calculate the attention activities of a GALA module as $\mathbf{A}_{h,w,c} = \zeta\left(a_c(\boldsymbol{G}^*_{h,w,c} + \boldsymbol{S}^*_{h,w,c}) + m_c(\boldsymbol{G}^*_{h,w,c} \cdot \boldsymbol{S}^*_{h,w,c})\right)$, where the activation function ζ is set to the $\tanh$ function, which squashes activities in the range $[-1, 1]$. In contrast to other bottom-up attention modules, which use a sigmoidal function to implement a soft form of excitation and inhibition, our selection of $\tanh$ gives a GALA module the additional ability to dis-inhibit bottom-up feature activations from **U** and flip the signs of its individual unit responses. Attention is applied by F_{scale} as $\mathbf{U}' = \mathbf{U} \odot \mathbf{A}$.

3.2 RESNET-50 IMPLEMENTATION

We validated the GALA approach by embedding it within a ResNet-50 (He et al., 2016). We identified 6 mid- to high-level feature layers in ResNet-50 to use with GALA (layers 24, 27, 30, 33, 36, 39; each of which belong to the same ResNet-50 processing block), since these will in principle encode visual features that are qualitatively similar to the object-parts highlighted in ClickMe maps (see Fig. 2A for an example of such parts). Each GALA module was applied to the final activity in a dense path of a residual module in ResNet-50. At this depth in the ResNet, GALA attention activity maps had a height and width of 14×14. The residual layer's "shortcut" activity maps were added to this GALA-modulated activity to allow the ResNet to flexibly adjust the amount of attention applied to feature activities. Table 2 in the Appendix shows that the accuracy of our re-implementations of ResNet-50 (He et al., 2016) and SE-ResNet-50 (Hu et al., 2017) trained with randomly initialized weights on ILSVRC12 is on par with published results. Incorporating our proposed GALA module into the ResNet-50 (*GALA-ResNet-50 no ClickMe*) offers a small improvement over the SE-ResNet-50. As we will see in section 4, the benefits of GALA are much greater on smaller datasets and when we add attention supervision.

4 CO-TRAINING GALA WITH CLICKME MAPS

To this point, we have described the ClickMe dataset, which contains human-derived feature importance maps for ILSVRC12. We have also introduced the GALA module for learning local- and global-attention during object recognition. In this section we describe a method for supervising GALA with ClickMe maps, and the affect this has on model performance and interpretability.

We use ClickMe maps to supervise GALA module attention by introducing an additional loss. Let $\mathcal{L}_C$ denote the cross-entropy between activity from model M with input $\mathbf{X}$ and class label y. ClickMe maps are resized with bicubic interpolation to be the same height and width as a GALA module activity $\mathbf{A}^l(\mathbf{X})$ at layer $l \in \mathbf{L}$, the set of layers where the GALA module is applied. We denote the resized ClickMe map for this input as $R^l(\mathbf{X})$. We reduced the depth of each column in $\mathbf{A}^l(\mathbf{X})$ to 1 by setting them to their column-wise L_2 norm. Units in $R^l(\mathbf{X})$ (ClickMe maps) and $\mathbf{A}^l(\mathbf{X})$ (GALA activity) are transformed to the same range by normalizing each by their L_2 norms. ClickMe map supervision for a GALA module is scaled by λ and combined with cross-entropy into a global loss:

$$\mathcal{L}_T\left(\mathbf{X}, y\right) = \mathcal{L}_C(M(\mathbf{X}), y) + \lambda \sum_{l \in \mathbf{L}} \left\| \frac{R^l(\mathbf{X})}{\|R^l(\mathbf{X})\|_2} - \frac{\mathbf{A}^l(\mathbf{X})}{\|\mathbf{A}^l(\mathbf{X})\|_2} \right\|_2 \tag{1}$$

This formulation jointly optimizes a model for both object classification and predicting ClickMe maps from input images (the latter loss is referred to in Fig. 3 as $L_{clickmaps}$).

4.1 MODEL EVALUATION

We evaluated our approach for supervising GALA with ClickMe maps by partitioning the ClickMe dataset into separate folds for training, validation, and testing. We set aside approximately 5% of the dataset for validation (17,841 images and importance maps), another 5% for testing (17,581 images and importance maps), and the rest for training (329,036 images and importance maps). Each ClickMe split contained exemplars from all 1,000 ILSVRC12 categories. Training and validation splits are used in the analyses below to optimize the GALA training routine, whereas the test split is set aside for evaluating model performance and interpretability.

4.2 TRADE-OFF BETWEEN RECOGNITION PERFORMANCE AND CLICKME MAP PREDICTION

We investigated the trade-off between maximizing object categorization accuracy and predicting ClickMe maps (i.e., learning a visual representation which is consistent with that of human observers). We performed a systematic analysis over different values of the hyperparameter λ, which scaled the magnitude of the ClickMe map loss (Eq. 1), while recording object classification accuracy and the similarity between ground-truth ClickMe maps and model attention maps (Fig. 7 in Appendix). This analysis demonstrated that both object categorization and ClickMe map prediction improve when $\lambda = 6$. We use this hyperparameter value to train *GALA-ResNet-50 with ClickMe maps* in subsequent experiments.

4.3 MODEL ACCURACY

We compared model performance on the test split of the ClickMe dataset (Table 1). Here, we report classification accuracy and the fraction of human ClickMe map variability explained by feature maps at the model layer where GALA was applied (where 100 is the observed inter-participant reliability; see Appendix). High scores on explaining human ClickMe map variability indicates that a model selects similar features as humans for recognizing objects. We found that the GALA-ResNet-50 was more accurate at object classification than either the ResNet-50 or the SE-ResNet-50. We also found that all models that incorporated attention were better at predicting ClickMe maps than a baseline ResNet-50. The most notable gains in performance came when ClickMe maps were used to supervise GALA-ResNet-50 training, which improved its classification performance and fraction of explained human ClickMe map variability.

We verified the effectiveness of ClickMe maps for co-training GALA with two controls, one of which tested the importance of detailed feature selections in ClickMe maps (see Fig. 2A for examples of

	top-1 err	top-5 err	maps
SE-ResNet-50	66.17	42.48	64.36**
ResNet-50	63.68	40.65	43.61
GALA-ResNet-50 no ClickMe	53.90	31.04	64.21**
GALA-ResNet-50 w/ ClickMe	**49.29**	**27.73**	**88.56****

Table 1: Top-1 and top-5 classification error of networks along with the fraction of human ClickMe map variability explained by their features (maps; 100 corresponds to the average similarity between human ClickMe maps). Performance is reported on the test set of ClickMe. ** denotes p <0.01 (statistical testing captures the proportion of image feature maps that exceed the null inter-participant reliability score; see Appendix for details).

how these maps emphasize certain object parts over others), while the other tested whether a GALA module is necessary for a model to benefit from ClickMe supervision. For our first control, we trained a GALA-ResNet-50 on coarse bounding-box annotations of objects (see Appendix for details on how these bounding boxes were generated). The second control tested if ClickMe maps could directly improve feature learning in ResNet-50 architectures, without the aid of the GALA module (see Appendix for details on the training routine). In both cases, we found that the GALA-ResNet-50 trained with ClickMe maps outperformed the controls (Table 3 in Appendix). In other words, the detail in ClickMe maps improves GALA performance, and ClickMe maps applied directly to model feature encoding did not help performance.

As an additional analysis, we tested if ClickMe maps could still improve model performance if they were only available for a subset of the training set. We trained models on the entire ILSVRC12 training set and provided ClickMe supervision on images for which it was available (test accuracy was measured on the ILSVRC12 validation set). Here too the GALA-ResNet-50 with ClickMe map supervision was more accurate than all other models (Table 4 in Appendix).

4.4 Model interpretability

Because GALA-ResNet-50 networks were trained "from scratch" on the ClickMe dataset, we were able to visualize the features selected by each for object recognition. We did so on a set of 200 images that was not included in ClickMe training, for which we had multiple participants supply ClickMe maps. We visualized features by calculating "smoothed" gradient images (Smilkov et al., 2017), which suppresses visual noise in gradient images. Including ClickMe supervision in GALA-ResNet-50 training yielded gradient images which highlighted features that were qualitatively more local and consistent with those identified by human observers (Fig. 4), emphasizing object parts such as facial features in animals, and the tires and headlights of cars. By contrast, the GALA-ResNet-50 trained without ClickMe maps placed more emphasis on the bodies of animals and cars as well as their context.

Our ClickMe map loss formulation requires reducing the dimensionality of the GALA attention volume A to a single channel. We can visualize these "reduced attention maps" to see the image locations GALA modules learn to select (Fig. 4). Strikingly, attention in the GALA-ResNet-50 trained with ClickMe maps, virtually without exception, focuses either on a single important visual feature of the target object class, or segments the figural object from the background. This effect persists in the presence of clutter and occlusion (Fig. 4, fourth and last row of GALA w/ ClickMe maps). In comparison, some object features can be made out in the attention maps of a GALA-ResNet-50 trained without ClickMe maps, but there is no such localization, and the maps themselves are far more difficult to interpret. The interpretability of the attention used by these GALA modules is reported in Table 1: GALA-ResNet-50 trained with ClickMe selects more similar features to human observers than the GALA-ResNet-50 trained without ClickMe (the respective fraction of explained ClickMe map variability is 88.56 vs. 64.21, p <0.001 according to a randomization test on the difference in per-image scores between the models, as in Edgington, 1964).

Attention in the GALA-ResNet-50 trained with ClickMe supervision also was capable of selecting objects in images from a different dataset than ILSVRC. Without additional training, the model's attention localized foreground object parts in Microsoft COCO 2014 (Lin et al., 2014), despite the

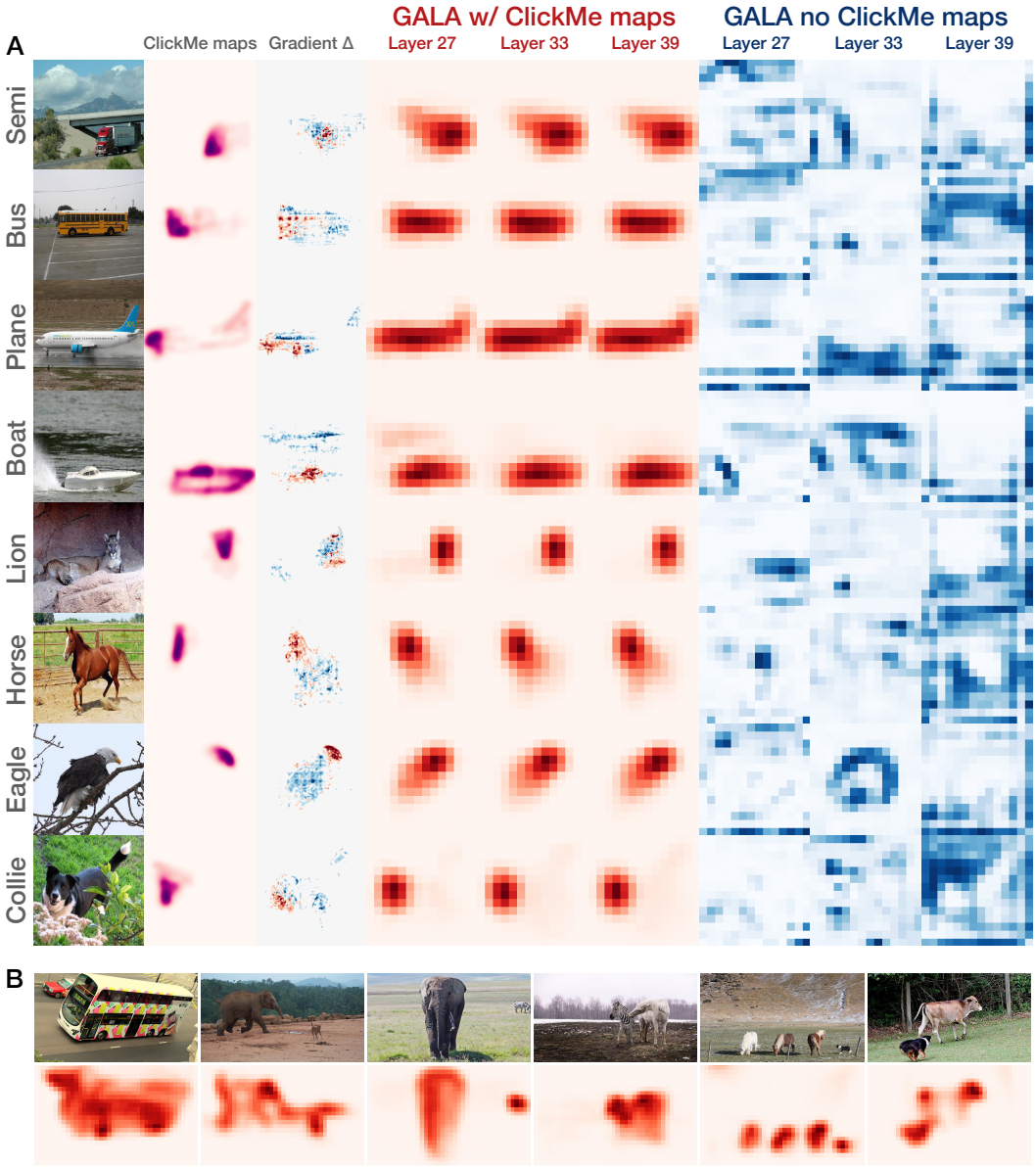

Figure 4: A GALA-ResNet-50 trained with ClickMe supervision uses visual features that are more similar to those used by human observers than a GALA-ResNet-50 trained without such supervision. (A) ClickMe maps (images were held out from the training set) highlight object parts that are deemed important by human observers. The difference between normalized smoothed gradient images (Smilkov et al., 2017) from each network shows relative feature preferences between networks (Gradient Δ). Image pixels preferred by GALA-ResNet-50 with ClickMe are red, and those preferred by a GALA-ResNet-50 without ClickMe are blue, depicting the preference for local features of the former over the latter. The column-wise L_2 norm of each network's GALA modules reveals highly interpretable object and part-based attention for the ClickMe GALA-ResNet-50 (in red) vs. less interpretable and more diffuse attention for the vanilla GALA-ResNet-50 (in blue). (B) The GALA-ResNet-50 with ClickMe map training learns attention from ILSVRC12 that transfers to Microsoft COCO 2014 (zero-shot; see Fig. 8 for more examples). The attention maps, which locate multiple objects at once, are sampled from the final ResNet layer in which GALA is applied (#39).

qualitative differences between this dataset and ILSVRC (multiple object categories, higher resolution than ILSVRC12; see Fig. 8 for additional exemplars). We quantified the interpretability of GALA-

ResNet-50 attention on a subset of the Microsoft COCO 2017 detection challenge validation set, which contained object categories also in ILSVRC12 (over 2,000 images; see Appendix for details). On these images, we measured interpretability by calculating the intersection-over-union (IOU) of an attention map for an image with its ground truth object segmentation masks from COCO (Zhou et al., 2017). By this metric, attention from the GALA-ResNet-50 trained with ClickMe supervision is significantly more interpretable than attention from the same model without ClickMe supervision (0.26 IOU vs. 0.03 IOU, p <0.001 according to a randomization test detailed in Appendix).

5 DISCUSSION

We have described a novel global-and-local attention (GALA) module and demonstrated the benefit of using supervision to teach DCNs where to attend. We first described the collection of the ClickMe dataset aimed at supplementing ImageNet with nearly a half-million human-derived attention maps. The approach was validated using human psychophysics by demonstrating the sufficiency of ClickMe features for rapid visual categorization: on average, human observers were able to reach ceiling accuracy with only 6% of the total pixels made visible derived from the most selected ClickMe locations. These results indicate that `ClickMe.ai` may also provide novel insights into human vision with a measure of feature diagnosticity that goes beyond classic saliency measures. While a detailed analysis of the ClickMe features falls outside the scope of the present study, we expect a more systematic analysis that moves beyond identifying what features are selected to also measure when they are selected (Cichy et al., 2016; Ha and Eck, 2017) will aid our understanding of the different attention mechanisms responsible for the selection of diagnostic image features. We release all the ClickMe data, including not only nearly a half-million attention maps, but also the associated timing of human behavioral decisions, with the hope that it will spur interest from other researchers.

We also extended the squeeze-and-excitation (SE) module which constituted the building block of the winning architecture in the ILSVRC17 challenge. We trained an SE-ResNet-50 on a reduced amount of data ($\sim 300K$ samples) and found that the architecture overfits compared to a standard ResNet-50. We have found that the proposed GALA-ResNet-50, however, significantly increases accuracy in this regime and cuts down top-5 error by $\sim 25\%$ over both ResNet-50 and SE-ResNet-50. In addition, we described an approach to co-train GALA using ClickMe supervision and cue the network to attend to image regions that are diagnostic to humans for object recognition. The routine casts ClickMe map prediction as an auxiliary task that can be combined with a primary visual categorization task. We found a trade-off between learning visual representations that are more similar to those used by human observers vs. learning visual representations that are more optimal for ILSVRC. The proper trade-off resulted in a model with better classification accuracy and more interpretable visual representations (both qualitatively and according to quantitative experiments on the ClickMe dataset and Microsoft COCO images).

While recent advancements in DCNs have led to models that perform on par with human observers in basic visual recognition tasks, there is also growing evidence of qualitative differences in the visual strategies that they employ (Saleh et al., 2016; Ullman et al., 2016; Eberhardt et al., 2016; Linsley et al., 2017). It remains an open question whether these discrepancies arise because of mechanistic differences during visual inference or because of more mundane differences in the way they are trained. That it is possible to drive a modern DCN towards learning more human-like representations with proper cuing to diagnostic image regions during training suggests that the observed differences may reflect different training regimens rather than different inference strategies. In particular, DCNs lack explicit mechanisms for perceptual grouping and figure-ground segmentation which are known to play a key role in the development of our visual system (Johnson, 2001; Ostrovsky et al., 2009). Such processes alleviate the need to learn to discard background clutter through statistical regularities learned via the presentation of millions of training samples as is the case for DCNs. In the absence of figure-ground mechanisms, DCNs are compelled to associate foreground objects and their context as single perceptual units. This leads to DCN representations that are significantly more distributed compared to those used by humans (Linsley et al., 2017). We hope that this work will catalyze interest in the development of novel training paradigms that leverage the plethora of visual cues (depth, motion, etc) available for figure-ground segregation in order to substitute for the human supervision used here for co-training GALA.

REFERENCES

S. Bell, C. Lawrence Zitnick, K. Bala, and R. Girshick. Inside-outside net: Detecting objects in context with skip pooling and recurrent neural networks. In *Proceedings of the IEEE Conference on Computer Vision and Pattern Recognition*, pages 2874–2883, 2016.

M. Biparva and J. Tsotsos. STNet: Selective tuning of convolutional networks for object localization. In *The IEEE International Conference on Computer Vision (ICCV)*, volume 2, 2017.

C. Cao, X. Liu, Y. Yang, Y. Yu, J. Wang, Z. Wang, Y. Huang, L. Wang, C. Huang, W. Xu, D. Ramanan, and T. S. Huang. Look and think twice: Capturing Top-Down visual attention with feedback convolutional neural networks. In *2015 IEEE International Conference on Computer Vision (ICCV)*, pages 2956–2964, Dec. 2015.

L. Chen, H. Zhang, J. Xiao, L. Nie, J. Shao, W. Liu, and T. S. Chua. SCA-CNN: Spatial and Channel-Wise attention in convolutional networks for image captioning. In *2017 IEEE Conference on Computer Vision and Pattern Recognition (CVPR)*, pages 6298–6306, July 2017.

R. M. Cichy, A. Khosla, D. Pantazis, A. Torralba, and A. Oliva. Comparison of deep neural networks to spatio-temporal cortical dynamics of human visual object recognition reveals hierarchical correspondence. *Sci. Rep.*, 6:27755, June 2016.

A. Das, H. Agrawal, L. Zitnick, D. Parikh, and D. Batra. Human attention in visual question answering: Do humans and deep networks look at the same regions? In *Proceedings of the 2016 Conference on Empirical Methods in Natural Language Processing*, pages 932–937, Stroudsburg, PA, USA, 2016. Association for Computational Linguistics.

J. Deng, J. Krause, and L. Fei-Fei. Fine-Grained crowdsourcing for Fine-Grained recognition. In *2013 IEEE Conference on Computer Vision and Pattern Recognition*, pages 580–587, June 2013.

J. Deng, J. Krause, M. Stark, and L. Fei-Fei. Leveraging the wisdom of the crowd for Fine-Grained recognition. *IEEE Trans. Pattern Anal. Mach. Intell.*, 38(4):666–676, Apr. 2016.

S. Eberhardt, J. Cader, and T. Serre. How deep is the feature analysis underlying rapid visual categorization? In *Neural Information Processing Systems*, 2016.

E. S. Edgington. Randomization tests. *The Journal of psychology*, 57:445–449, Apr. 1964.

T. M. Gureckis, J. Martin, J. McDonnell, A. S. Rich, D. Markant, A. Coenen, D. Halpern, J. B. Hamrick, and P. Chan. psiturk: An open-source framework for conducting replicable behavioral experiments online. *Behav. Res. Methods*, 48(3):829–842, Sept. 2016.

D. Ha and D. Eck. A neural representation of sketch drawings. Apr. 2017.

K. He, X. Zhang, S. Ren, and J. Sun. Deep residual learning for image recognition. In *Computer Vision and Pattern Recognition*, 2016.

J. Hu, L. Shen, and G. Sun. Squeeze-and-Excitation networks. Sept. 2017.

L. Itti and C. Koch. Computational modelling of visual attention. *Nat. Rev. Neurosci.*, 2(3):194–203, 2001.

L. Itti, G. Rees, and J. K. Tsotsos. *Neurobiology of attention*. Academic Press, 2005.

S. Jetley, N. A. Lord, N. Lee, and P. H. S. Torr. Learn to pay attention. Apr. 2018.

M. Jiang, S. Huang, J. Duan, and Q. Zhao. SALICON: Saliency in context. In *2015 IEEE Conference on Computer Vision and Pattern Recognition (CVPR)*, pages 1072–1080, June 2015.

S. P. Johnson. Visual development in human infants: Binding features, surfaces, and objects. *Vis. cogn.*, 8(3-5):565–578, June 2001.

T. Judd, K. Ehinger, F. Durand, and A. Torralba. Learning to predict where humans look. *CVPR*, 2009.

A. Kovashka, O. Russakovsky, L. Fei-Fei, and K. Grauman. Crowdsourcing in computer vision. Nov. 2016.

T.-Y. Lin, M. Maire, S. Belongie, L. Bourdev, R. Girshick, J. Hays, P. Perona, D. Ramanan, C. Lawrence Zitnick, and P. Dollár. Microsoft COCO: Common objects in context. May 2014.

D. Linsley, S. Eberhardt, T. Sharma, P. Gupta, and T. Serre. What are the visual features underlying human versus machine vision? Jan. 2017.

V. Mnih, N. Heess, A. Graves, and K. Kavukcuoglu. Recurrent models of visual attention. *Advances in Neural Information Processing Systems 27*, 27:1–9, 2014.

H. Nam, J. W. Ha, and J. Kim. Dual attention networks for multimodal reasoning and matching. In *2017 IEEE Conference on Computer Vision and Pattern Recognition (CVPR)*, pages 2156–2164, July 2017.

T. V. Nguyen, Q. Zhao, and S. Yan. Attentive systems: A survey. *Int. J. Comput. Vis.*, 126(1):86–110, Jan. 2018.

A. Oliva and A. Torralba. The role of context in object recognition. *Trends Cogn. Sci.*, 11(12): 520–527, 2007.

Y. Ostrovsky, E. Meyers, S. Ganesh, U. Mathur, and P. Sinha. Visual parsing after recovery from blindness. *Psychol. Sci.*, 20(12):1484–1491, Dec. 2009.

J. Park, S. Woo, J.-Y. Lee, and I.-S. Kweon. Bam: Bottleneck attention module. *CoRR*, abs/1807.06514, 2018.

B. Patro and V. P. Namboodiri. Differential attention for visual question answering. Apr. 2018.

B. Saleh, A. Elgammal, and J. Feldman. The role of typicality in object classification: Improving the generalization capacity of convolutional neural networks. Feb. 2016.

T. Serre, A. Oliva, and T. Poggio. A feedforward architecture accounts for rapid categorization. *Proceedings of the National Academy of Sciences of the United States of America*, 104(15): 6424–6429, Apr. 2007.

K. Shanmuga Vadivel, T. Ngo, M. Eckstein, and B. S. Manjunath. Eye tracking assisted extraction of attentionally important objects from videos. In *Proceedings of the IEEE Conference on Computer Vision and Pattern Recognition*, pages 3241–3250, 2015.

D. Smilkov, N. Thorat, B. Kim, F. Viégas, and M. Wattenberg. SmoothGrad: removing noise by adding noise. June 2017.

M. Stollenga, J. Masci, F. Gomez, and J. Schmidhuber. Deep networks with internal selective attention through feedback connections. *arXiv preprint arXiv: . . .*, page 13, 2014.

I. Sutskever, J. Martens, G. Dahl, and G. Hinton. On the importance of initialization and momentum in deep learning. In *International Conference on Machine Learning*, pages 1139–1147, Feb. 2013.

S. Thorpe, D. Fize, and C. Marlot. Speed of processing in the human visual system. *Nature*, 381 (6582):520–522, June 1996.

A. Torralba, A. Oliva, M. S. Castelhano, and J. M. Henderson. Contextual guidance of eye movements and attention in real-world scenes: the role of global features in object search. *Psychol. Rev.*, 113 (4):766–786, Oct. 2006.

S. Ullman, L. Assif, E. Fetaya, and D. Harari. Atoms of recognition in human and computer vision. *Proc. Natl. Acad. Sci. U. S. A.*, 113(10):2744–2749, Mar. 2016.

L. von Ahn, R. Liu, and M. Blum. Peekaboom: A game for locating objects in images. In *Proceedings of the SIGCHI Conference on Human Factors in Computing Systems*, CHI '06, pages 55–64, New York, NY, USA, 2006. ACM.

C. Vondrick, H. Pirsiavash, A. Oliva, and A. Torralba. Learning visual biases from human imagination. In C. Cortes, N. D. Lawrence, D. D. Lee, M. Sugiyama, and R. Garnett, editors, *Advances in Neural Information Processing Systems 28*, pages 289–297. Curran Associates, Inc., 2015.

F. Wang, M. Jiang, C. Qian, S. Yang, C. Li, H. Zhang, X. Wang, and X. Tang. Residual attention network for image classification. In *2017 IEEE Conference on Computer Vision and Pattern Recognition (CVPR)*, pages 6450–6458, July 2017.

Q. You, H. Jin, Z. Wang, C. Fang, and J. Luo. Image captioning with semantic attention. In *2016 IEEE Conference on Computer Vision and Pattern Recognition (CVPR)*, pages 4651–4659, June 2016.

S. Zagoruyko and N. Komodakis. Paying more attention to attention: Improving the performance of convolutional neural networks via attention transfer. Dec. 2016.

B. Zhou, D. Bau, A. Oliva, and A. Torralba. Interpreting deep visual representations via network dissection. Nov. 2017.

APPENDIX

ADDITIONAL CLICKME STATISTICS

The game was launched on February 1st, 2017 and closed on September 24th, 2017. Over this period, 25 contests were used to drive traffic to the site by rewarding top-scoring players with gift cards. Participants were given usernames to track their performance and were allowed to play as many game rounds as they wanted. More than 90% of these participants played more than one image. The distribution of number of participants per image is shown in Fig. 5.

Around 5% of the images were skipped by participants because of poor image quality or an incorrect class label. The CNN correctly recognized object images in about half of the trials that were played (47% of all images) for which participants received points. In total, we recorded over 35M bubbles, producing 472,946 ClickMe maps on 196,499 unique images.

ClickMe maps typically highlight local image features, emphasizing certain object parts over others (Fig. 6). For instance, ClickMe maps for animal categories (top row) are nearly always oriented towards facial components even when these are not prominent (e.g., snakes). In general, we also found that ClickMe maps for inanimate objects tended to exhibit a front-oriented bias, with distinguishing parts such as engines, cockpits, and wheels receiving special attention.

INTER-RATER RELIABILITY OF THE CLICKME MAPS

We first verified that despite the large scale of ClickMe, the collected attention maps displayed strong regularity and consistency across participants. We calculated the rank-ordered correlation between ClickMe maps from two randomly selected players for an image. These maps were blurred with a 49x49 kernel (the square of the bubble radius in the ClickMe game) to facilitate the comparison and reduce the influence of noise associated with the game interface. Repeating this procedure for 10,000 different images and taking the average of these per-image correlations revealed a strong average inter-participant reliability of $\rho = 0.58$ (p <0.001), meaning that the kinds of features participants bubbled during game play tend to be stereotyped. We report the similarity between a model's feature attention maps and humans as a ratio of this value $\frac{\rho_{model}}{\rho_{human}}$, and refer to this as the "Fraction of human ClickMe map variability". We also derived a null inter-participant reliability by calculating the correlation of ClickMe maps between two randomly selected players on two randomly selected images. Across 10,000 randomly paired images, the average null correlation was $\rho_r = 0.18$, reinforcing the strength of the observed reliability. Below, we calculate p values for correlations between model features and ClickMe maps as the proportion of per-image correlation coefficients that are less than this value.

RELIABILITY BETWEEN CLICKME AND CLICKATIONARY MAPS

ClickMe was inspired by the Clicktionary game (Linsley et al., 2017), which has two human partners play together to identify important visual features. A small set of 10 images from that game were provided to us by the authors, and also used in ClickMe. A comparison of the reliability in attention maps for these images between the two games supports an evaluation of the extent to which ClickMe models the mechanics of Clicktionary. The correlation between ClickMe and Clicktionary maps for these 10 images was high ($\rho_r = 0.59$, p <0.001; statistical testing with randomization tests (Edgington, 1964)) and on par with the inter-experiment reliability reported for the Clicktionary game (Linsley et al., 2017). This suggests that ClickMe identifies similar visual features as Clicktionary, albeit in a much more efficient way, by swapping out one human partner with a DCN.

OBSERVERS DID NOT ADOPT A DCN-SPECIFIC STRATEGY

Importantly, participants did not adopt strategies to find visual features that were more important to their DCN partners than to other humans. A sensitivity analysis of this sort is impossible given the mechanics and statistics of gameplay: (1) Participants on average played fewer rounds than the number of object categories in ClickMe (380 vs. 1,000). (2) ClickMe participants were not aware of how their clicked regions were revealed to their DCN partners (Fig. 1). (3) The top-200 most frequent players were just as likely to elicit correct responses from their DCN on the first half of their

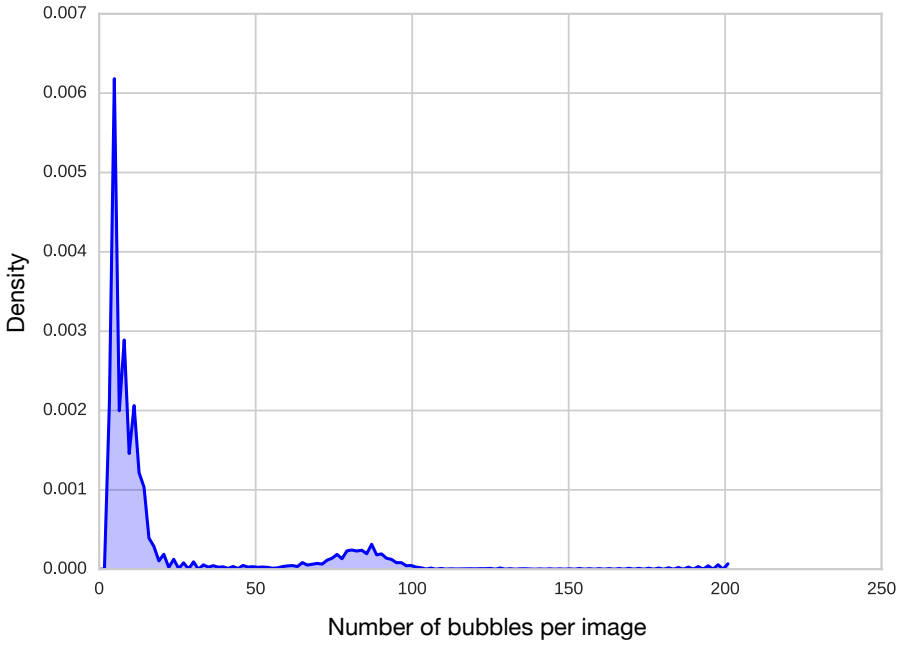

Figure 5: Distribution of participants per ClickMe map.

game rounds as on the second half, meaning these "expert" participants did not learn anything about features preferred by DCNs (53.64% vs. 53.61%; $t(199) = 0.04$, n.s. according to randomization test). (4) These same players did not show learning effects over a shorter timescale either: they were just as accurate on the first ten trials as they were on their second set of ten trials (49.30% vs. 52.20%, n.s. according to randomization test). In addition, as we will describe below, the similarity between ClickMe visual features selected by human participants is significantly greater than the similarity between human and DCN features. This means that participants were choosing features that they found important for recognition, and that these features were strongly stereotyped between players.

PSYCHOPHYSICS METHODS

Stimulus generation We created a "stochastic" flood-fill algorithm which we applied to a phase-scrambled version of a ClickMe object image to reveal increasingly larger image regions. First, the image pixel given highest importance by a ClickMe map was identified. Second, the algorithm expanded this region anisotropically, with a bias towards pixels with higher attention scores. The revealed region was set to the center of the image to ensure that participants did not have to foveate to see important image parts and to prevent the spatial layout to affect the results. Separate image sets were generated by this procedure for ClickMe and Salicon saliency maps. Participants viewed images masked by one type of map or the other, but never both to prevent memory effects. Participants saw each unique exemplar only once in a randomly selected masking configuration. The total number of pixels in the attention maps for a given image was equalized between ClickMe and saliency maps. Original images were sampled from 4 target and 4 distractor categories: bird, zebra, elephant, and cat; table, couch, refrigerator, and umbrella.

Psychophysics experiment In each experiment trial, participants viewed a sequence of events overlaid onto a white background: (i) a fixation cross was first displayed for a variable time (1,100–1,600ms); (ii) followed by the test stimulus for 400ms; (iii) and an additional 150ms of response time. In total, participants were given 550ms to view the image and press a button to judge its category (feedback was provided when response times fell outside this time limit). Participants were instructed to categorize the object in the image as fast and accurately as possible by pressing the "s" or "l" key, which were randomly assigned across participants to either the target or distractor category. Similar paradigms and timing parameters yielded reliable behavioral measurements of pre-attentive visual system processes (e.g., Eberhardt et al., 2016). The experiment began with a

brief training phase to familiarize participants with the paradigm. Afterwards, participants were given feedback on their categorization accuracy at the end of each of the five experimental blocks (16 images per block).

Experiments were implemented with the psiTurk framework (Gureckis et al., 2016) and custom javascript functions. Each trial sequence was converted to an HTML5-compatible video format to provide the fastest reliable presentation time possible in a web browser. Videos were preloaded before each trial to optimize the reliability of experiment timing within the web browser. A photo-diode was used to verify stimulus timing was consistently accurate within 10ms across different operating system, web browser, and display type configurations. Images were sized at 256×256 pixels, which is equivalent to a stimulus size between approximately $5^o - 11^o$ across a likely range of possible display and seating setups participants used for the experiment.

Two participant groups completed this experiment: one which viewed images with parts revealed according to ClickMe maps, and the other with parts revealed according to their Salicon-derived salience. Statistical testing between group performance with randomization tests Edgington (1964), which compared the performance between ClickMe vs. Salicon groups at every "percentage of image revealed by feature source" bin (x-axis in Fig. 2). A null distribution of "no difference between groups" at that bin was constructed by randomly switching participants' group memberships (e.g., a participant who viewed ClickMe mapped images was called a Salicon viewer instead), and calculating a new difference in accuracy between the two groups. This procedure was repeated 10,000 times for every bin, and the proportion of these randomized scores that exceeded the actual observed difference was taken as the *p*-value.

GALA-ResNet-50 training

In our experiments, ClickMe maps were blurred with a 49x49 kernel (the square of the bubble radius in the ClickMe game), before training to aid in convergence. Object image and ClickMe importance map pairs were passed through the network during training and augmented with identical random crops, and left-right flips. Models were trained for 100 epochs and weights were selected that yielded the best validation accuracy. All models were implemented in Tensorflow and were trained "from scratch" with weights drawn from a scaled normal distribution. We used SGD with Nesterov momentum (Sutskever et al., 2013) and a piece-wise constant learning rate schedule that decayed by $1/10$ after 30, 60, 80, and 90 epochs of training.

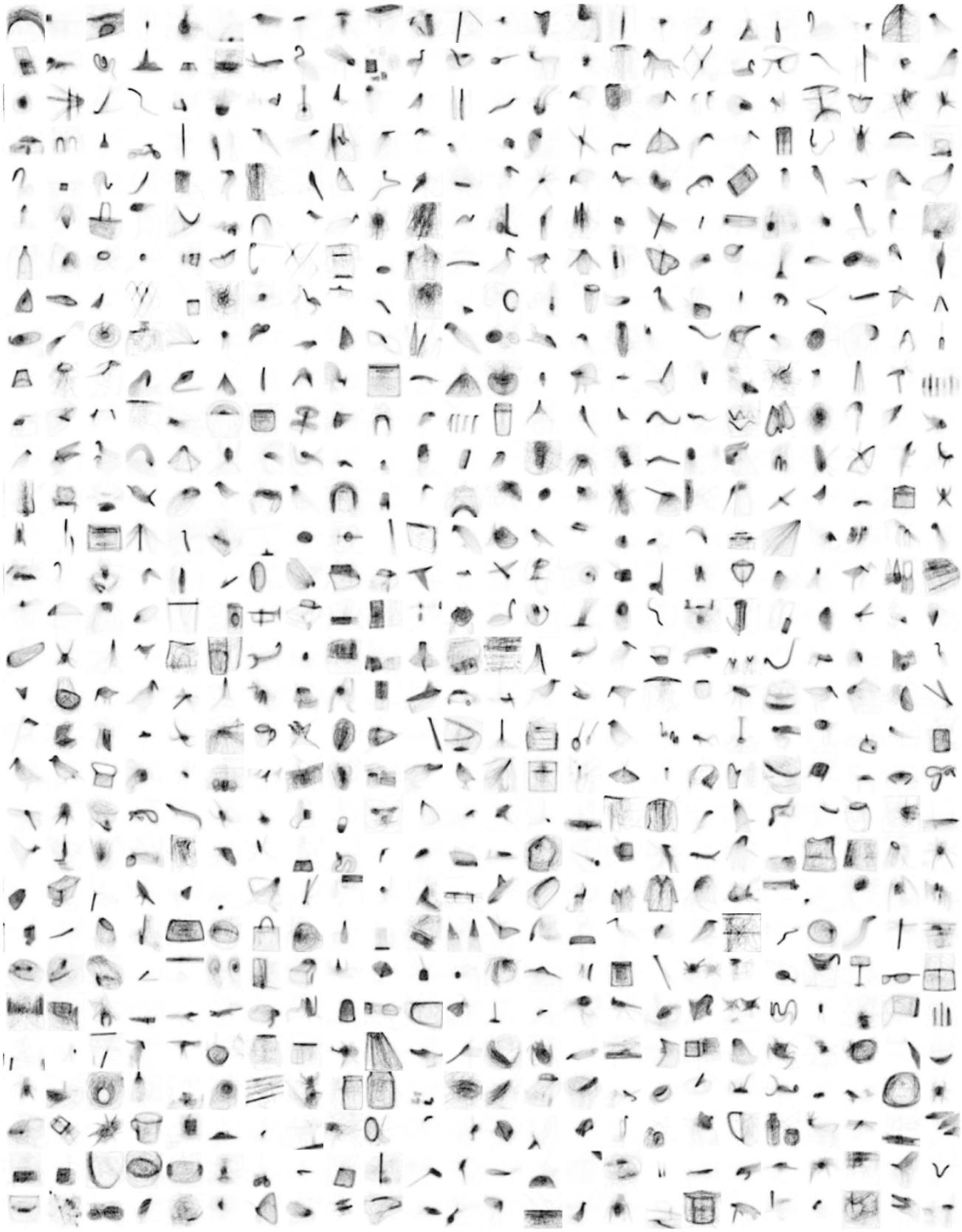

Figure 6: ClickMe map exemplars.

Models trained on full versions of ILSVRC12 (Table 2 and Table 4) were trained with Google TPUs on Google Cloud Virtual Machines. The large amount of TPU VRAM enabled models in these experiments to be trained with batches of 1,024 images. Bicubic interpolation operations used for resizing ClickMe maps were replaced with biliear interpolation on the TPUs, since the former is not supported. Models trained on the ClickMe subset of ILSVRC12 were trained with TITAN X Pascal GPUs (Table 1 in the main text and Table 3). Because of memory constraints, these models were trained with batches of 32 images. See `https://github.com/<user>/GALA_ClickMe`[2] for a reference implementation.

TRADE-OFF BETWEEN OBJECT RECOGNITION ACCURACY AND CONSISTENCY OF ATTENTION MAPS WITH HUMANS

We investigated the trade-off between maximizing object categorization accuracy and predicting ClickMe maps (i.e., learning a visual representation which is consistent with that of human observers). We performed a systematic analysis over different values of the hyperparameter λ, which scaled the magnitude of the ClickMe map loss, while recording object classification accuracy the similarity between ClickMe maps and model attention maps. Attention maps were derived from networks as the feature column-wise L_2 norms of activity from the final layer of GALA or SE attention (Zagoruyko and Komodakis, 2016). Model attention map similarity with ClickMe maps was measured with rank-order correlation. At each value of λ that was tested, five models were trained for 100 epochs, and weights that optimized accuracy on the validation ClickMe dataset were selected (Fig. 7). This analysis demonstrated that both object categorization and ClickMe map prediction improve when $\lambda = 6$.

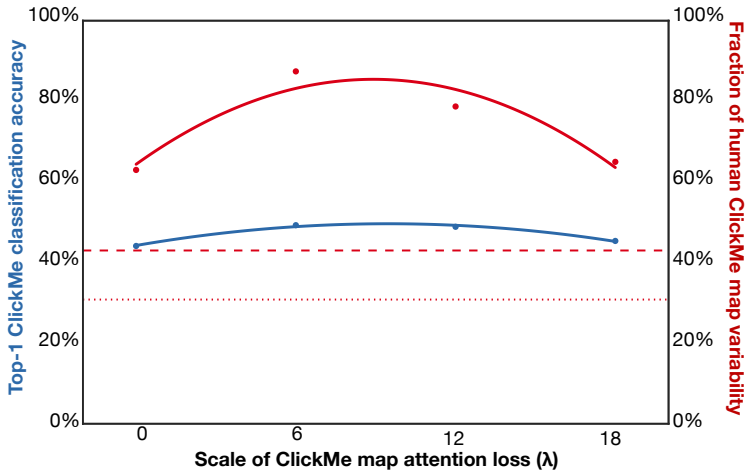

Figure 7: Training the GALA-ResNet-50 with ClickMe maps improves object classification performance and drives attention towards features selected by humans. We screened the influence of ClickMe maps on training by measuring model accuracy after training on a range of values of λ, which scales the contribution of ClickMe maps on the total model loss. A model optimized only for object recognition uses features that explain 62.96% of variability in human ClickMe maps, which is consistent with a ResNet-50 trained without attention (dashed red line). Incorporating ClickMe maps in the loss yields a large improvement in predicting ClickMe maps (87.62%) as well as classification accuracy. The fraction of explained ClickMe map variability for each model is plotted as its ratio to the human inter-rater reliability, and the dotted red line depicts the floor inter-rater reliability (shuffled null).

GALA-RESNET-50 VALIDATION

We benchmarked GALA-ResNet-50 versus a vanilla ResNet-50 and a ResNet-50 with SE attention (Hu et al., 2017) on the validation split of the ILSVRC12 challenge dataset (Table 2). These models

[2]This github link will be updated after the review period, to protect anonymity.

	Reference		Ours	
	top-1 err.	top-5 err.	top-1 err.	top-5 err.
ResNet-50 (He et al., 2016)	24.70	7.80	23.88	6.86
SE-ResNet-50 (Hu et al., 2017)	23.29	6.62	23.26	6.55
GALA-ResNet-50 no ClickMe	-	-	**22.73**	**6.35**

Table 2: ILSVRC12 validation set accuracy for published reference models (Hu et al., 2017) and our re-implementations. Models were evaluated on 224 $\times$ 224 image crops from the original ILSVRC12 encoded into sharded TFRecords (`gs://imagenet_data/train`).

	top-1 err	top-5 err	Maps
SE-ResNet-50	66.17	42.48	64.36**
ResNet-50	63.68	40.65	43.61
ResNet-50 w/ ClickMe	61.32	41.42	31.18
GALA-ResNet-50 w/ b. boxes	58.14	35.17	76.42**
GALA-ResNet-50 no ClickMe	53.90	31.04	64.21**
GALA-ResNet-50 w/ ClickMe	**49.29**	**27.73**	**88.56****

Table 3: Networks' classification error and fraction of explained human ClickMe map variability on 224 $\times$ 224 center crops from the ClickMe test set. The dataset can be downloaded from `ClickMe.ai/about`. ** denotes p <0.01 (statistical testing captures the proportion of feature maps that exceed null inter-participant reliability, detailed in *Inter-rater reliability of the ClickMe maps*).

were trained on the original version of ILSVRC12. Our implementation is consistent with published references, and we find that the GALA-ResNet-50 outperforms the other models[3].

As discussed in the main text, the GALA-ResNet-50 excelled on the ClickMe subset of ILSVRC12 (Table 3). The GALA-ResNet-50 was more accurate and better able to predict human attention maps than either the SE-ResNet-50 or the ResNet-50. This model's performance was improved dramatically when it was co-trained with ClickMe maps, which cut down top-5 error by $\sim 25\%$ over both ResNet-50 and SE-ResNet-50.

To understand the effectiveness of ClickMe supervision when it is only available for a subset of all images in a dataset, we also tested these models on a preparation of the full ILSVRC12 for the ClickMe game. Once again, the GALA-ResNet-50 trained with ClickMe maps outperformed all other models in classification performance (Table 4).

GALA-ResNet-50 controls

Two control experiments evaluated (1) the effectiveness of ClickMe maps for attention supervision, and (2) whether attention modules were even needed for a model benefit from this form of supervision.

We first measured the importance of fine-grained annotations in ClickMe maps for supervising GALA attention. To do this, we compared the GALA-ResNet-50 with ClickMe maps to one trained on "bounding boxes" derived from these maps. Bounding boxes were created by drawing a rectangle over the ClickMe map that spanned its spatial extent. In practice, these bounding boxes do not necessarily line up neatly with classical bounding boxes drawn around objects for localization tasks. However, it still provides useful information about the resolution at which attention supervision is needed. The GALA-ResNet-50 trained with ClickMe maps outperformed one trained with these bounding boxes on both the ClickMe subset of ILSVRC12 (Table 3) and our preparation of the ILSVRC12 (Table 4).

We also tested if ClickMe maps can directly supervise feature learning in residual networks. This involved replacing the ClickMe map attention loss with one that minimized the L_2 distance between ClickMe maps and activity volumes from a ResNet-50 during object classification training (this loss

[3]We observed an identical pattern of results and approximately equal performance for both the classic pre- and more recent "post-activation" flavors of ResNet-50 (He et al., 2016).

	top-1 err	top-5 err
ResNet-50	28.60	9.65
SE-ResNet-50	27.52	8.91
GALA-ResNet-50 no ClickMe	27.28	8.78
GALA-ResNet-50 w/ b. boxes	27.24	8.80
GALA-ResNet-50 w/ ClickMe	**26.17**	**8.12**

Table 4: Networks trained on the full ILSVRC12 training set, with ClickMe supervision on only a subset of these images ($\sim$16% of all images). This experiment demonstrates that ClickMe maps are not needed for all training samples to benefit from ClickMe supervision. Network classification error is reported on 224 $\times$ 224 center crops from ILSVRC12 validation[5]. The dataset can be download at `ClickMe.ai/about`.

was applied to the same layers as the attention models above; Table 3, ResNet-50 w/ ClickMe). This model performed comparably to a normal ResNet-50, but was less accurate than the GALA-ResNet-50 with ClickMe maps.

INTERPRETABLE ATTENTION

We measured the interpretability of attention maps employed by GALA-ResNet-50 models trained with versus without ClickMe map supervision on a subset of images in the Microsoft COCO 2017 object detection challenge that contained animal and vehicle categories also present in ILSVRC12 (2,055 images; this criteria was used because these models were trained on ILSVRC12). For each of the selected images, we also collected animal and vehicle segmentation masks from the challenge. Thus, this amounted to a large "zero-shot" test of the interpretability of GALA model attention.

Each COCO image was resized to 480×640 pixels, and passed through the GALA-ResNet-50 trained with ClickMe and the GALA-ResNet-50 trained without ClickMe. Attention activities were extracted from the final GALA module in each module, and as was described in the main text, processed for visualization by setting attention columns at every spatial location to their L_2 norm, transforming the $H \times W \times C$ (corresponding to volume height, width, and channels) attention volume to $H \times W \times 1$. Because of subsampling in the ResNet-50, the height and width of the resulting attention mask was less than the input images. This was corrected by resizing these maps to 480×640 pixels.

We first visualized attention maps from the GALA-ResNet-50 models by using them as the transparency channel for their corresponding COCO images (a random subset is depicted in Fig. 8). There are striking regularities in the features selected by GALA attention when it is trained with ClickMe maps: important animal parts, such as faces and tails are consistently emphasized; as are vehicle parts like windshields and wheels (Fig. 8, middle mosaic). By contrast, GALA attention trained without ClickMe maps is much more distributed and less interpretable on these images, and highlights a combination of background and foreground elements (Fig. 8, bottom mosaic).

We quantified attention map interpretability with an approach inspired by Zhou et al. (2017), which was used to quantify the interpretability of deep network representations. For each image, we normalized attention maps from the two GALA models to the range of $[0, 1]$, then thresholded these maps to only include pixels with a score greater than 0.5. These attention maps were next processed to have the same number of these above-threshold pixel locations, to support a fair comparison of the two models. These above-threshold pixel locations were paired with an image's COCO segmentation masks to calculate an intersection-over-union (IOU) score, which measured the likelihood that a model's attention selected animal or vehicle parts versus background locations. Applying this procedure to all 2,055 COCO images yielded per-image scores in the range of $[0, 1]$. Comparing the average score of the two models revealed that ClickMe map supervision significantly improves the interpretability of GALA-ResNet-50 attention: GALA-ResNet-50 trained with ClickMe map supervision interpretability is 0.26, whereas GALA-ResNet-50 trained with ClickMe map supervision interpretability is 0.03. Furthermore, the difference between the two is statistically significant according to a randomization test (Edgington, 1964), in which the observed average difference is compared to a null distribution of average differences constructed by randomly flipping the signs of the per-image difference scores over 10,000 iterations (p <0.001).

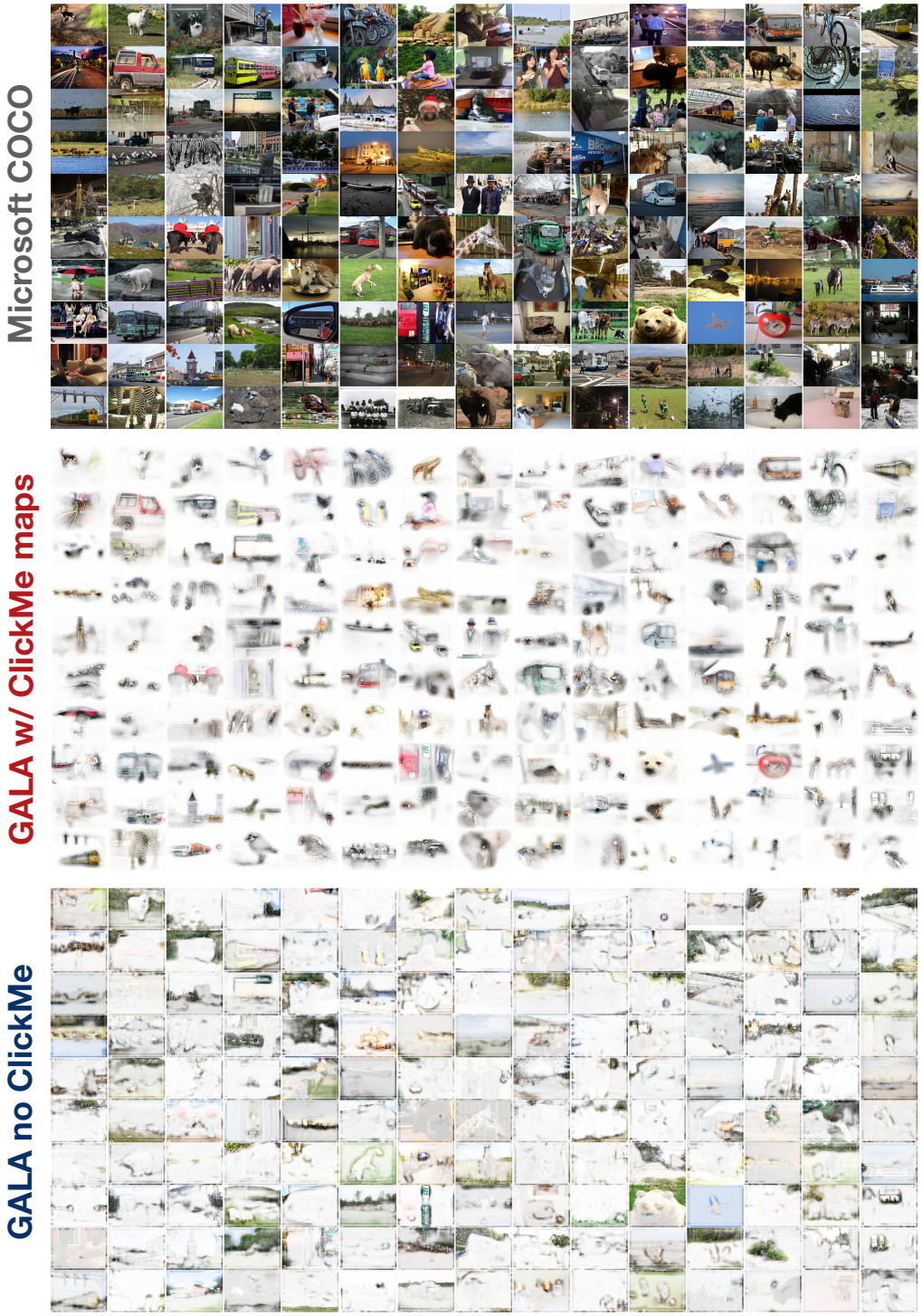

Figure 8: Exemplars from the validation set of the Microsoft COCO 2017 detection challenge (zoom in for detail). The top panel depicts a random selection from a subset of these images that depicted object categories also found in ILSVRC12. In the middle panel, each of these images is shown with the transparency set to the attention map it yielded in a GALA-ResNet-50 trained with ClickMe map supervision. Opaque parts indicate features that this GALA attended to, and transparent parts are ones that it ignored; this emphasizes animal parts like faces and tails, and vehicle parts like wheels and windshields. The bottom panel shows the same visualization using attention maps from a GALA-ResNet-50 trained without ClickMe map supervision. Here, attention is distributed and less interpretable.